Proceedings of CONF-MCEE 2026 Symposium: Advances in Sustainable Aviation and Aerospace Vehicle Automation
DOI: 10.54254/2755-2721/2026.KA29643

Improvement of Low Frequency Sound Absorption in a Room

Neil Wang

Choate Rosemary Hall, Wallingford, USA
chrakeoverwatch@gmail.com

Abstract. Low-frequency noise (LFN) poses significant challenges in noise control due to its long wavelengths and ability to penetrate barriers. This study introduces a novel metamaterial-based absorber optimized for low-frequency sound attenuation using a multicoiled structure. The theoretical foundation is established through an equivalent electrical-acoustic circuit representation, leading to the development of an impedance-matching design. The metamaterial's performance is validated using Finite Element Analysis (FEA) simulations incorporating thermoviscous acoustic interactions and experiments. The results demonstrate high absorption efficiency at 50 Hz, with a total structure thickness of only 13 mm. A case study on an open duct system confirms that incorporating multiple absorption modules enhances noise reduction, with up to 21 dB attenuation observed. These findings highlight the effectiveness of the proposed metamaterial for compact and efficient low-frequency noise control applications.

Keywords: metamaterial, simulation, impedance, subwavelenth

1. Introduction

Environmental noise pollution has become a significant public health concern, with the World Health Organization (WHO) highlighting its detrimental effects on human well-being. Among various types of noise pollution, low-frequency noise (LFN), typically in the range of 10 Hz to 160 Hz, is particularly problematic. Studies have shown that LFN exposure can cause sleep disturbances, cognitive impairment, cardiovascular problems, and stress-related illnesses [1,2]. Unlike higher-frequency sounds, which can be easily absorbed or blocked, LFN is more challenging to control due to its long wavelengths, which enable it to penetrate walls and other structural barriers effectively. Research indicates that LFN can travel long distances with minimal attenuation due to its low absorption in common building materials, further amplifying its impact on human health and well-being [3,4]. This characteristic makes LFN a pervasive issue, affecting both urban and rural environments.

One of the most common sources of LFN is bass-heavy music played in residential spaces, such as living rooms. While music is intended to be an enjoyable experience, the accompanying low-frequency components can lead to significant disturbances, including discomfort and potential health effects. Studies have shown that prolonged exposure to intense LFN can contribute to respiratory issues and ear discomfort, making it imperative to find effective mitigation strategies [1].Current low-frequency sound absorption solutions primarily rely on passive materials, such as

© 2025 The Authors. This is an open access article distributed under the terms of the Creative Commons Attribution License 4.0 (https://creativecommons.org/licenses/by/4.0/).

DOI: 10.54254/2755-2721/2026.KA29643

Helmholtz resonators, membrane-type absorbers, micro-perforated materials, and subwavelength metamaterials [2-4]. Helmholtz resonators function by trapping sound waves in a cavity and dissipating energy through resonance, effectively attenuating specific low-frequency bands [5]. Membrane-type absorbers operate by utilizing a vibrating membrane backed by an air cavity, which absorbs sound energy through controlled resonance [6]. Micro-perforated materials achieve noise reduction through a network of perforations that create viscous losses, converting acoustic energy into heat [7]. Subwavelength metamaterials, an emerging class of engineered structures, leverage specially designed unit cells to manipulate wave propagation, offering ultra-thin and broadband low-frequency noise absorption [8]. These materials are designed to target specific frequency ranges through resonant absorption or impedance-matching mechanism. Despite their effectiveness, these traditional approaches suffer from limitations such as bulky designs, high cost and narrow bandwidth absorption, thereby failing to provide a universally efficient, space-saving, and health-conscious solution for mitigating LFN in residential environments [9].

To address these challenges, this study aims to explore an alternative approach to LFN attenuation that is fibre-free, thin, and space-efficient while maintaining high sound absorption performance at low frequencies. Section 2 establishes the theoretical framework by drawing an analogy between electrical circuits and acoustic systems, leading to an equivalent circuit model that provides insight into impedance matching and optimal absorption characteristics. Section 3 details the tuning mechanism that enables resonance frequency adjustment while maintaining structural compactness. Finite Element Analysis (FEA) is then employed in Section 4 to validate the theoretical model, incorporating thermoviscous acoustic interactions to assess the pressure distribution and absorption efficiency. Finally, Section 5 presents a case study evaluating the performance of the metamaterial in an open duct system, demonstrating its potential for real-world noise reduction applications.

2. Methodology

The proposed subwavelength absorber is designed to target low-frequency noise by going beyond the limits of conventional quarter-wavelength absorbers, which require impractically thick structures. Its design, often referred to as a multicoiled metasurface (MCM), combines three main elements: a top plate with a small hole acting as the neck, an aperture connecting the surface to the cavity, and a set of labyrinthine passages that form a large coiled cavity (see Figure 1).

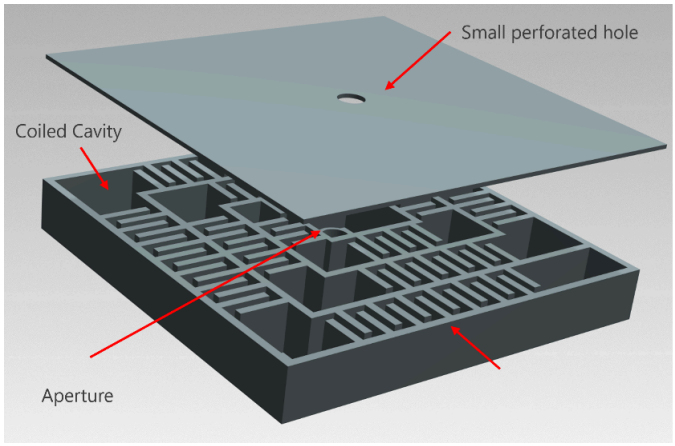


Figure 1. Typical design of a subwavelength metamaterial

DOI: 10.54254/2755-2721/2026.KA29643

The physical principle of the absorber can be understood using the mass–spring analogy. The air in the neck behaves like an oscillating mass, while the air inside the coiled cavity acts as an elastic spring. When sound waves enter through the small hole, they set the neck air into motion, compressing and expanding the cavity air. This back-and-forth motion produces resonance between the “mass” of the neck air and the “spring” of the cavity air.

The resonance frequency is governed by the relationship between the neck geometry and the cavity volume. Extending the labyrinthine path increases the effective cavity volume, which reduces the stiffness of the air spring. As the spring becomes softer, the resonance frequency shifts downward. In this way, a compact labyrinth structure can resonate with very long wavelengths, far below what its physical thickness would normally allow.

This mechanism enables strong absorption at low frequencies. Once sound enters the coiled channels, viscous and thermal losses at the narrow walls dissipate acoustic energy into heat. To broaden the absorption bandwidth, multiple cavities of different sizes can be combined or thin resistive layers can be added, ensuring efficient performance across a wider range of frequencies.

Although physically thin, the labyrinthine design creates a large effective acoustic volume and tunes the resonance into the low-frequency range. As a result, the structure behaves as if it were acoustically much thicker, making it highly effective for attenuating low-frequency noise in a compact form. The multicoiled geometry further optimizes the internal space, reducing thickness while maintaining high absorption efficiency.

The perforated plate and aperture play a crucial role in fine-tuning impedance matching. They regulate the airflow resistance at the entrance, ensuring that incoming sound energy couples effectively into the cavity rather than being reflected. As air flows through the small apertures, frictional losses dissipate part of the acoustic energy, while the coiled cavity traps the remaining energy, extending the interaction time and lowering the resonance frequency. The labyrinthine passages inside the chamber further lengthen the acoustic path, enhancing absorption at extremely low frequencies without increasing the overall thickness of the metasurface.

By combining these mechanisms, the multicoiled metasurface overcomes the physical limitations of conventional absorbers, delivering enhanced low-frequency attenuation in a compact design. This approach opens the way for ultra-thin, high-performance noise-control materials that are practical for both residential and commercial applications.In order to design the metamaterial properly, the concept of the surface impedance need to be introduced. The acoustic behavior of the metasurface can be described in terms of its surface impedance Zs, defined as the ratio of sound pressure to particle velocity at the surface of the absorber. Physically, it’s essentially the acoustic opposition a surface gives to sound energy entering.

It has been widely accepted that absorption performance depends on both resistance and reactance. The sound absorption coefficient cannot exceed 1, as this represents complete absorption. For maximum absorption, the numerator should reach its highest possible value while the denominator remains as small as possible. This condition is satisfied when the surface impedance is perfectly matched to that of air: the real part equals the characteristic resistance of air, and the reactive terms cancel out. Under these impedance-matching conditions, reflection at the surface disappears, all incident acoustic energy enters the resonator, and the energy is dissipated through viscous and thermal mechanisms.

3. Theoretical modelling

The modeling of the proposed metamaterial is founded on the equivalence between electrical circuits and acoustic systems, which arises because both are governed by second-order differential

DOI: 10.54254/2755-2721/2026.KA29643

equations. In the aqcoustic domain, the motion of air in the neck and cavity of a resonator can be described by Newton's second law and Boyle's law, while in the electrical domain, the behavior of current and voltage in an RLC circuit is described by Kirchhoff's laws. The mathematical similarity between these governing equations allows an acoustic resonator to be expressed as a lumped-element RLC network.

In the electrical case, Kirchhoff's voltage law applied to a series RLC circuit gives

$$L\frac{d^2i}{dt^2} + R\frac{di}{dt} + \frac{1}{C}i = \frac{dV}{dt} \tag{1}$$

where i is the current, V is the applied voltage, L is inductance, R is resistance, and C is capacitance. This is a linear, second-order ordinary differential equation describing the balance between energy storage in the inductor, energy storage in the capacitor, and energy dissipation in the resistor.

A directly analogous equation can be derived for an acoustic Helmholtz resonator. The air slug in the neck of length l and cross-sectional area A has an effective mass, which is given by

$$m_a = \frac{\rho l}{A} \tag{2}$$

Applying Newton's law gives

$$m_a\frac{d^2u}{dt^2} + R_a\frac{du}{dt} + \frac{1}{C_a}u = \frac{dp}{dt} \tag{3}$$

where u is the volume velocity (the time derivative of volume displacement), $\mathrm{R_a}$ is the acoustic resistance associated with viscous and thermal losses, $\mathrm{C_a}$ is the acoustic compliance of a cavity of volume, and p is the acoustic pressure excitation. This equation has exactly the same form as the RLC differential equation.

The equivalence can be illustrated by network diagrams: in the electrical case, voltage drives a series RLC loop, while in the acoustic case, pressure drives an equivalent system composed of acoustic mass (the neck), acoustic resistance (viscous losses), and acoustic compliance (the cavity). In both cases, the dynamics are determined by a second-order ODE, which predicts resonance when the inertial term and the compliant term cancel, leaving only resistive dissipation.

This explicit second-order formulation shows that the acoustic resonator behaves exactly like an RLC circuit. The resonance frequency, bandwidth, and absorption characteristics of the metamaterial can therefore be tuned in the same way electrical engineers tune circuits: by adjusting the effective mass through the neck geometry, altering the compliance through cavity volume, and controlling the resistance through aperture and wall losses. This framework provides both a clear physical explanation and a systematic design methodology for creating high-performance subwavelength absorbers.

DOI: 10.54254/2755-2721/2026.KA29643

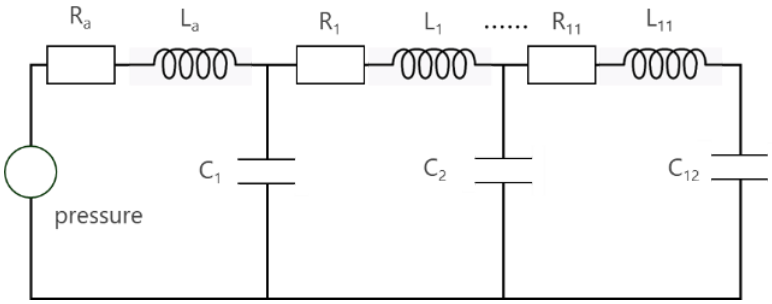


Figure 2. Equivalent RLC circuit model for a subwavelength metamaterial

The circular aperture, perforated plate, and labyrinthine structures contribute to the acoustic resistance and inductance of the system, while the cavity gaps contribute to acoustic capacitance (see Figure 2). Using Crandall's theory, the acoustic impedance per unit length for an infinite aperture is calculated. Given that the aperture has a considerable height, thermal-viscous losses must be considered. The acoustic resistance Ra and inductance Ma of the circular aperture are given by [10]:

$$R_a = \sqrt{2\omega\rho_0\eta} \tag{4}$$

$$M_a = \frac{4A}{\pi d^2}\left[\sqrt{2\omega\rho_0\eta} - \frac{2\rho_0 c sin\frac{k_c k_a}{2}}{\omega(\gamma-(\gamma-1)\Psi_h)\Psi_r}\right] \tag{5}$$

where ω is the angular frequency, η is the air's dynamic viscosity, kc is the complex wave number, and ha is the aperture height. The terms Ψh and Ψr describe thermal and viscous fields within the aperture [11], while A represents the integral metasurface area.

The labyrinthine structures divide the channel into multiple narrow coiled passages and cavities, where the width of labyrinthine passages is denoted by . The resistance and inductance associated with these structures are determined by:

$$R = \frac{h_c}{\pi d^3}\sqrt{2\mu\omega\rho_0} + 2\frac{\sqrt{2\mu\omega\rho_0}}{\pi d^2} + \frac{\rho_0 c_0}{\pi d^2}\left[1 - \frac{2J_1(2kd)}{2kd}\right] \tag{6}$$

$$M = \frac{l_b\rho_0}{S} \tag{7}$$

where lb is the total length, S is the total area of the channel, and J1 is the first-order Bessel function. The different cavity volumes within the system introduce varying acoustic capacitance values, calculated as:

$$C = \frac{V}{\rho_0 c_0^2} \tag{8}$$

where V is the cavity volume. Since the resistor and inductor are in series, while the capacitor C is in parallel and connected to the ground, the total acoustic impedance of the metamaterial is given by:

$$Z = \frac{1}{\frac{1}{Z_{Ra}+Z_{La}}+\frac{1}{Z_{C1}}} + \frac{1}{\frac{1}{Z_{R1}+Z_{L1}}+\frac{1}{Z_{C2}}} + \sum_{i=2}^{10}\frac{1}{\frac{1}{Z_{Ri}+Z_{Li}}+\frac{1}{Z_{Ci}}} + (Z_{R11}+Z_{L11}+Z_{C12}) \tag{9}$$

DOI: 10.54254/2755-2721/2026.KA29643

This formulation allows a comprehensive understanding of the impedance characteristics of the metamaterial, facilitating the design and optimization of ultra-thin acoustic absorbers with enhanced low-frequency performance.

By using this strategy, a metamaterial with a tuning frequency of approximately 50 Hz is designed. The detailed key dimensions of this structure are shown in Figure 3.

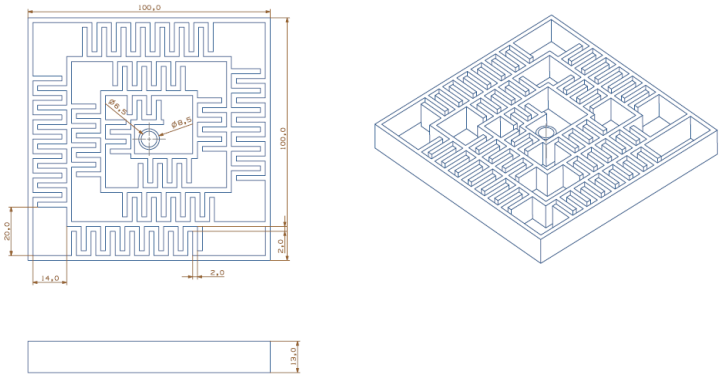


Figure 3. Key dimensions of the meta-structure

The resultant theoretical sound absorption coefficient is shown in Figure 4.

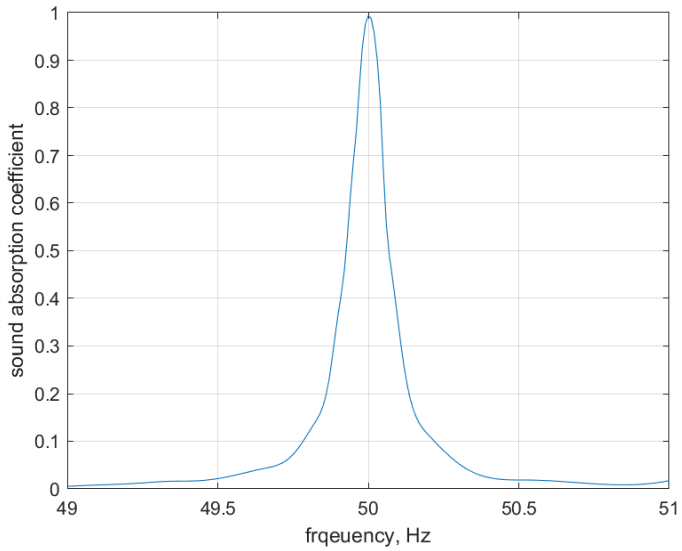


Figure 4. Theoretical sound absorption coefficient for designed meta-structure

4. Validation using finite element model

Finite Element Analysis (FEA) is employed to validate the theoretical model and to evaluate the sound absorption performance of the proposed metamaterial. The introduction of FEA is necessary because the theoretical modeling process inevitably involves certain simplifications and approximations. In particular, potential errors may arise from assumptions related to the end correction of the labyrinth path lengths, the effective cavity size, and the influence of the perforation holes in the plate. The numerical calculations are performed using the acoustic-thermoviscous acoustic interaction module in Simcenter 3D within the frequency domain. The effect of viscous

DOI: 10.54254/2755-2721/2026.KA29643

friction and heat transfer is incorporated into the model through the linearized compressible Navier–Stokes equation, the continuity equation, and the energy equation. Hard boundary conditions are imposed on the interfaces between air and solid materials due to the large impedance mismatch between them. An example configuration for this simulation is shown in Figure 5.

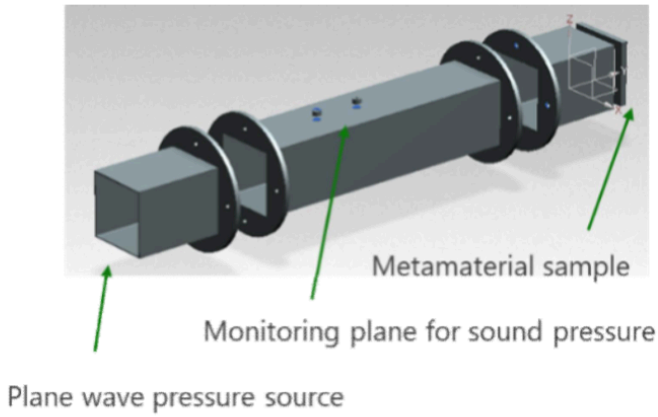


Figure 5. Configuration of the sound absorption coefficient simulation

Figure 6 shows that perfect absorption is achieved at 48 Hz with a total system thickness of 13 mm.

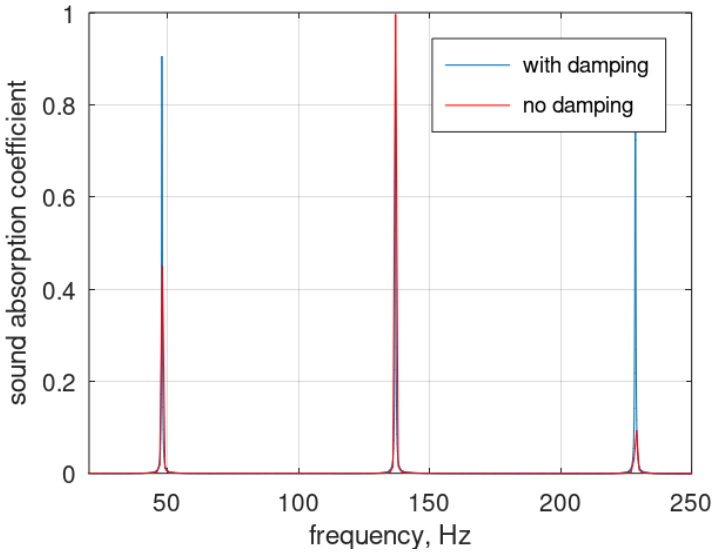


Figure 6. Sound absorption coefficient for this meta-structure

To further understand the physical absorption mechanisms, the acoustic pressure distribution inside the metamaterial at the resonant frequency (48 Hz) is analyzed (see Figure 7).

DOI: 10.54254/2755-2721/2026.KA29643

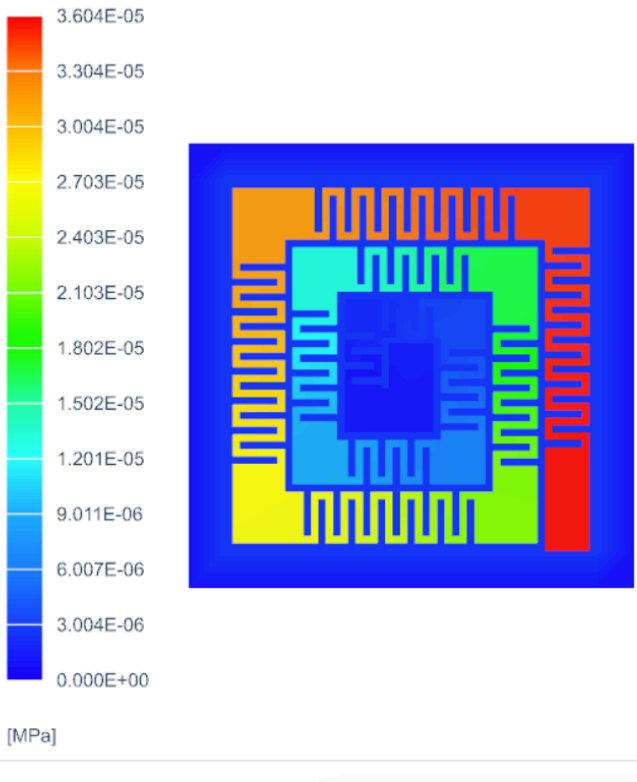


Figure 7. Sound pressure accumulation inside the meta-structure

The high acoustic pressure observed inside the multicoiled structure at resonance can be understood as energy being trapped within the labyrinth. This trapping effect is a direct consequence of impedance mismatch between the incident wave in the duct and the resonant mass–spring system formed by the neck air mass and the cavity compliance. At resonance, the impedance of the resonator approaches that of air, which minimizes reflection and allows the incident energy to enter the labyrinth. Once inside, the long coiled path ensures that the wave interacts repeatedly with the channel walls. The geometry effectively couples the acoustic wavelength with the equivalent stiffness of the cavity: when the incident wavelength is comparable to the resonant condition set by the labyrinth length, strong oscillations occur between the “mass” of the neck air and the “spring” of the cavity air.

This coupling allows energy to be stored temporarily inside the resonator. However, because the air is forced through narrow passages, viscous friction and thermal conduction at the boundaries continuously drain energy from the oscillating system. Instead of being released back into the duct as a reflected pressure wave, much of the energy is dissipated as heat. The labyrinth therefore serves as an acoustic sink: impedance matching ensures that sound energy enters, the mass–spring resonance couples the wave to the structure, and the extended channel length maximizes the dissipation process. The net effect is a significant reduction of the reflected wave amplitude in the duct and a corresponding increase in the absorption coefficient.

5. Prediction of sound reduction index for a duct with this meta-structure

To further evaluate the practical effectiveness of the metamaterial, a transmission loss simulation has been conducted in an open duct integrated with the designed metamaterial. This simulation aims to

DOI: 10.54254/2755-2721/2026.KA29643

quantify the impact of the metamaterial in reducing transmitted noise and improving overall sound attenuation. The analysis investigates different configurations, including variations in the number of absorption modules to determine their effect on noise reduction performance.

The configuration of the metastructure inside the rectangular duct is illustrated in Figure 8. In the simulation, a plane-wave particle velocity source was applied at one end of the duct to generate the incident acoustic field, while an anechoic boundary condition was imposed at the opposite end to eliminate reflections and simulate free-field radiation. The sound power levels at the inlet and outlet of the duct were then calculated, and their difference was used to evaluate the noise reduction achieved by incorporating the metamaterial. This approach provides a direct measure of the attenuation performance of the system by quantifying how much acoustic energy is dissipated as the wave propagates through the metastructure.

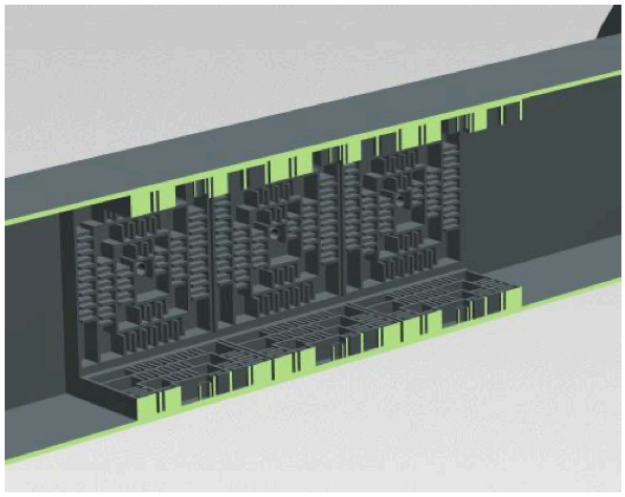
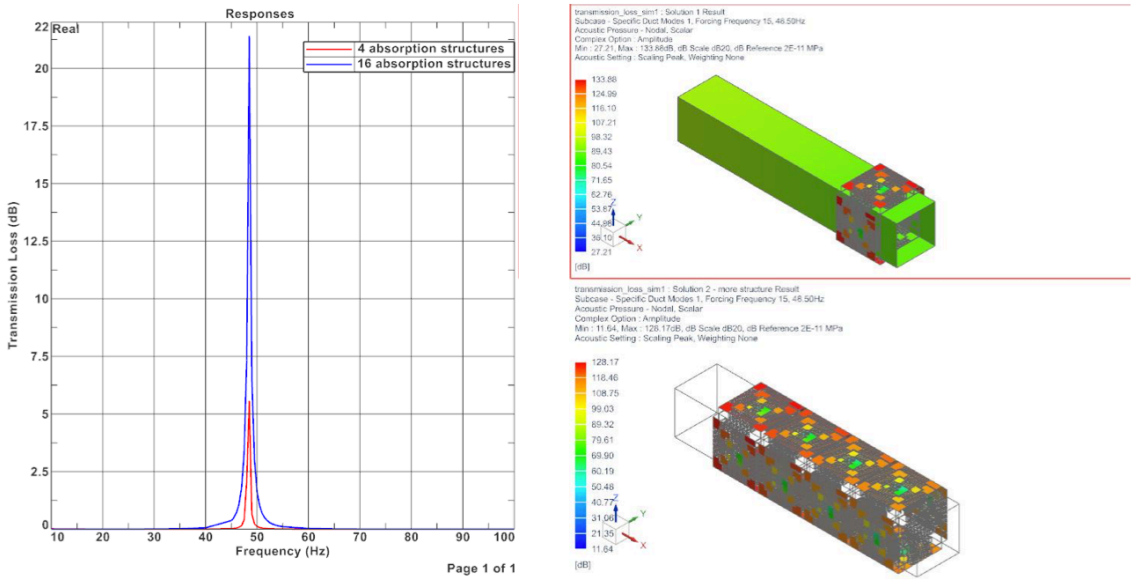


Figure 8. Configuration how the meta-structures incorporated into a rectangular duct

Figure 9 demonstrates that with four absorption modules, a noise reduction greater than 5 dB is achieved, while increasing the number of modules to sixteen enhances the noise reduction up to 21 dB. This trend indicates that a greater number of modules significantly improves absorption efficiency by providing increased interaction between the sound waves and the labyrinthine structure. The transmission loss spectra, as shown in the graph, highlight a sharp attenuation peak near 50 Hz, aligning well with the targeted resonance frequency of the metamaterial.

DOI: 10.54254/2755-2721/2026.KA29643



(a)transmission loss curve (b)pressure distribution at 48.5 Hz

Figure 9. Sound reduction index simulation results

Additionally, the simulation's pressure distribution results reveal how sound waves interact with the metamaterial within the duct. The absorption structures generate localized high-pressure zones, where energy dissipation is maximized through viscous and thermal losses. Comparisons between configurations with fewer and more modules illustrate that increased module density leads to more effective impedance matching and enhanced broadband absorption. These findings confirm that the metamaterial-based approach is capable of achieving significant noise reduction in open duct environments, demonstrating its potential for real-world acoustic applications.

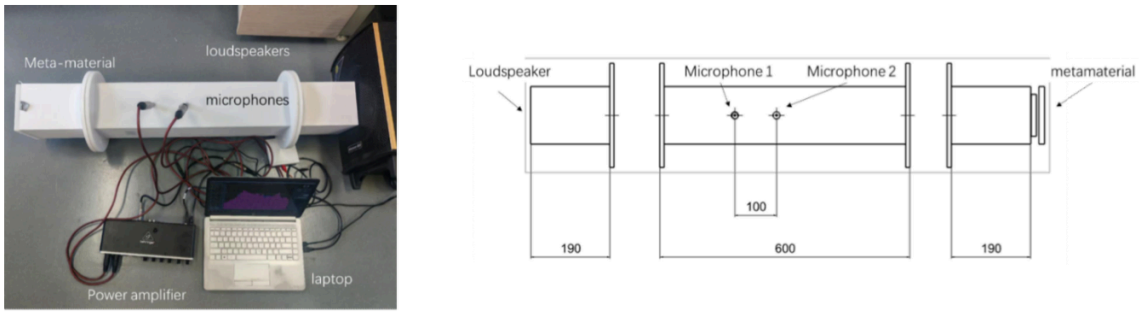
6. Experimental investigation of the sound absorption coefficient for the metamaterial

In order to evaluate the performance of the metamaterial, a dedicated test rig was developed to measure the normal-incidence sound absorption coefficient. Because the target frequency of the metamaterial is determined by its design, it is important to establish a standardized procedure for evaluating its absorption performance. In practical applications, the random-incidence absorption coefficient is often more representative of real-world scenarios, as it accounts for sound arriving from multiple directions. However, standardized normal-incidence measurements are still highly valuable, since they provide a consistent and repeatable method for characterizing materials and comparing their specifications. For this reason, the design and implementation of a controlled test configuration remain an essential step in verifying the acoustic performance of the proposed metamaterial.

The test rig is designed with a modular configuration so that it can later be reused for sound transmission experiments. As illustrated in Figure 10, the rig is divided into three main sections: the excitation section containing the loudspeaker, the microphone section, and the duct section for installing the metamaterial sample. The loudspeaker is mounted at one end of the duct, followed by a 190 mm excitation section to ensure the generation of a stable plane wave before reaching the microphone section. Two microphones are positioned 100 mm apart within a 600 mm central duct, allowing pressure measurements in accordance with the two-microphone transfer function method specified in ISO 10534-2. At the opposite end, a 190 mm mounting section accommodates the

DOI: 10.54254/2755-2721/2026.KA29643

metamaterial. An adapter is employed to eliminate the gap between the metamaterial sample and the duct walls, thereby ensuring accurate boundary conditions and minimizing acoustic leakage. The different parts of the rig are joined using flanges, with rubber sealing rings placed between them to guarantee airtight connections. This modular arrangement not only facilitates straightforward sample installation and replacement but also provides flexibility for adapting the rig to different experimental configurations. The detailed configuration of the test rig can be seen in Figure 10.



(a)layout (b)key dimensions

Figure 10. Test configuration of the impedance tube

The calculated normal incident sound absorption coefficient can be seen in Figure 11.

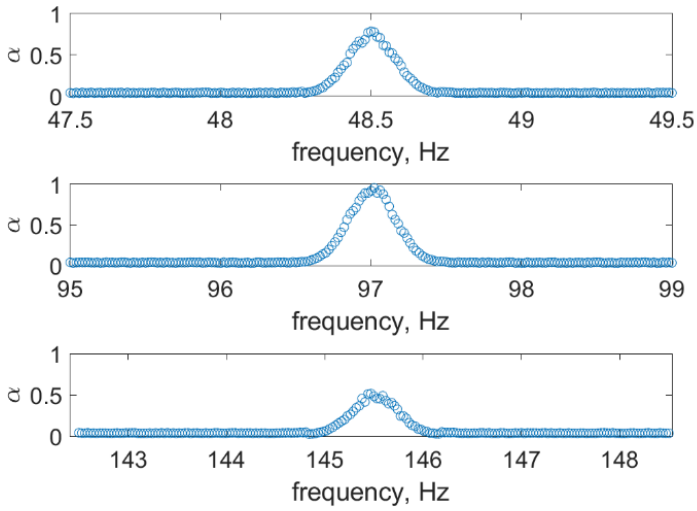


Figure 11. Normal incident sound absorption coefficient at given frequencies

As expected, a pronounced absorption peak is observed at 48.5 Hz, which is slightly shifted from the designed resonance frequency of 50 Hz. One of the primary reasons for this deviation lies in the geometry of the labyrinth. During the design stage, in order to accommodate the required cavity volume within the coiled layout, the cross-sectional area of the cavity had to be adjusted. This modification alters the effective compliance of the cavity, which in turn shifts the resonance frequency slightly below the targeted value. Moreover, this geometric adjustment also affects the distribution of acoustic mass and compliance, which contributes to a broader resonance bandwidth than initially predicted. As a result, the absorption peak not only appears at a slightly lower frequency but also exhibits a wider profile compared to the theoretical design.

DOI: 10.54254/2755-2721/2026.KA29643

The experimental absorption levels are still slightly offset from the simulation results. This discrepancy can largely be attributed to uncertainties in manufacturing. The minimum air channel width in the labyrinth is only 2 mm, and due to the limitations of 3D printing, maintaining precise dimensional accuracy is challenging. A tolerance of approximately 0.2 mm is common, which corresponds to nearly a 10–20% deviation in channel size. Such deviations directly affect the effective acoustic mass and compliance of the structure, thereby shifting the resonance frequency and altering the absorption performance. In addition to manufacturing tolerances, environmental conditions during testing may also contribute to the observed differences. The measurements were conducted in Shanghai during the summer, when the ambient temperature was around 40 °C. At such elevated temperatures, the speed of sound increases compared to standard conditions, which can also shift the absorption peaks to higher frequencies.

7. Experimental investigation of the transmission loss for a duct equipping with the metamaterial

To facilitate the installation of the metamaterial, a smaller duct was designed, allowing for easier handling and assembly. This compact duct configuration also makes it feasible to install multiple ducts in parallel for more flexible testing arrangements. In the present measurement campaign, twelve metamaterial units were installed inside the duct. This setup enables the evaluation of the overall noise reduction achieved by the metamaterials under more realistic operating conditions.

For this measurement, the microphone was positioned facing the outlet of the duct. Although this setup does not constitute a strict or fully precise measurement of the radiated sound power level, it nevertheless provides a useful indication of the noise reduction performance in this case. The results can therefore serve as a practical reference for evaluating the effectiveness of the metamaterial under the given test conditions.

Experiment results reveal that the absorber reduces the sound pressure significantly in several bands.

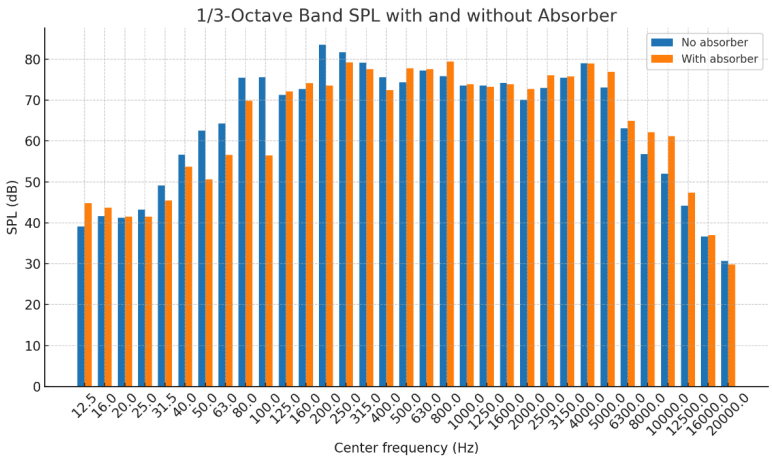


Figure 12. Sound reduction level difference with and without metamaterial

Figure 12 shows that the absorber performs very well at 50 Hz and 100 Hz, with reductions of almost 12 dB and 19 dB respectively. At 200 Hz, nearly 10 dB reduction is still observed. However, at 160 Hz, the result indicates a slight increase in level with the absorber installed. This discrepancy may be attributed to measurement uncertainty, possible structural resonances within the duct, or small dimensional inaccuracies in the metamaterial fabrication that affect tuning around this

DOI: 10.54254/2755-2721/2026.KA29643

frequency. A summary of the sound reduction with and without the meta material with targeted frequencies are shown in Table 1.

Table 1. Summary of the sound insertion loss for the targeted frequencies

Center Frequency (Hz)	No Absorber (dB)	With Absorber (dB)	Reduction (dB)
50	62.54	50.66	11.88
100	72.58	56.52	19.06
160	72.73	74.09	-1.36
200	83.51	73.57	9,94

An important observation from the 1/3-octave band analysis is the unexpected sound level increase around the 160 Hz band, rather than the anticipated reduction. This phenomenon can be explained by several mechanisms. First, the metamaterial behaves as a resonant system in which the mass of the neck and the compliance of the cavity form a mass–spring oscillator. Near resonance, strong coupling occurs between the incident wave and the resonator. If impedance matching is not achieved—for instance, due to insufficient resistive losses or small geometric deviations shifting the resonance frequency—the resonator may reradiate part of the stored energy back into the duct. Instead of being dissipated, this reemitted wave can interfere constructively with the incident sound, amplifying the measured sound level at the microphone location.

Another notable feature in the results is the unexpected reduction observed in the 63 Hz and 80 Hz 1/3-octave bands. Although the designed absorption peak was tuned to approximately 50 Hz, the measured data show additional attenuation at these slightly higher frequencies. This behavior can be explained by two factors. First, the labyrinthine structure inherently supports multiple resonances. While the fundamental resonance is governed by cavity volume and neck geometry, higher-order resonances can arise when the effective labyrinth path length corresponds to a fraction of the acoustic wavelength. These modes produce localized energy trapping and dissipation, which can explain the observed attenuation at 63 Hz and 80 Hz. Second, coupling between the metamaterial and duct acoustics may also contribute. At certain frequencies, the standing wave pattern in the duct can enhance energy flow into the absorber, broadening the effective frequency range of absorption.

At higher frequencies, discrepancies become more evident due to limitations of the two-microphone method. The plane-wave assumption is valid only below the cut-off frequency of the duct; once higher-order modes are excited, accuracy deteriorates. In addition, geometric tolerances inherent to 3D printing (on the order of ±0.2 mm in narrow 2 mm channels) can alter the effective acoustic path and introduce scattering, further degrading high-frequency performance. These factors collectively explain why deviations between experiment and simulation grow at higher frequencies, even though the low-frequency target is reproduced well.

Overall, the experimental results confirm that the proposed metamaterial achieves effective low-frequency noise reduction, with the absorption peak occurring close to the designed target. While discrepancies were observed—such as the unexpected reduction at 63 Hz and 80 Hz and the sound level increase near 160 Hz—these can be reasonably attributed to fabrication tolerances, measurement uncertainties, and structural resonances of the duct. Importantly, the general absorption trend agrees with theoretical predictions, and the overall performance remains of the same order of magnitude as the simulation. This validates the design concept and demonstrates the potential of the metamaterial for compact low-frequency noise control, while also highlighting areas for further refinement in both design and experimental methodology.

DOI: 10.54254/2755-2721/2026.KA29643

8. Conclusion

This study presents a novel metamaterial-based solution for low-frequency noise attenuation. By leveraging a multicoiled metastructure, the proposed absorber achieves high absorption efficiency at 50 Hz with a remarkably compact design. The theoretical foundation is established through an equivalent electrical-acoustic model, which is validated using Finite Element Analysis incorporating thermoviscous acoustic interactions. The results confirm the ability of the metamaterial to effectively dissipate acoustic energy through viscous and thermal losses, achieving near-perfect absorption at the targeted frequency. Furthermore, a case study on an open duct system demonstrates the scalability of the design, showing that increasing the number of absorption modules significantly enhances noise reduction performance. With reductions of up to 21 dB achieved, the study confirms that this metamaterial provides a promising approach for practical low-frequency noise control applications in engineering and industrial environments.

References

[1] Waye, K. Persson. Effects of Low Frequency Noise on Sleep. Noise and Health 6(23): p 87-91, Apr–Jun 2004.
[2] Schust M. Effects of low frequency noise up to 100 Hz [J]. Noise and Health, 2004, 6(23): 73-85.
[3] Leventhall HG. Low frequency noise and annoyance. Noise Health. 2004 Apr-Jun; 6(23): 59-72. PMID: 15273024..
[4] Shabalina E. The propagation of low frequency sound through an audience [M]. Logos Verlag Berlin GmbH, 2014.
[5] Gorain J, Padmanabhan C. Broadband low-frequency noise reduction using Helmholtz resonator-based metamaterial [J]. Noise Control Engineering Journal, 2021, 69(4): 351-363.
[6] Liao Y, Huang H, Chang G, et al. Research on low-frequency noise control of automobiles based on acoustic metamaterial [J]. Materials, 2022, 15(9): 3261.
[7] Zhao X, Wang X, Yu Y. Enhancing low-frequency sound absorption of micro-perforated panel absorbers by combining parallel mechanical impedance [J]. Applied Acoustics, 2018, 130: 300-304.
[8] Dal Poggetto V F. Bioinspired acoustic metamaterials: From natural designs to optimized structures [J]. Frontiers in Materials, 2023, 10: 1176457.
[9] El-Basheer T M, Mohamed H K. Recent progress in acoustical materials and noise control approach [J].
[10] Huang, X. Fang, X. Wang, B. Assouar, Q. Cheng, and Y. Li, “Acoustic perfect absorbers via spiral metasurfaces with embedded apertures, ” Appl. Phys. Lett.113(23), 233501 (2018).
[11] M. R. Stinson and E. A. G. Shaw, “Acoustic impedance of small, circular orifices in thin plates, ” J. Acoust. Soc. Am. 77(6), 2039–2042 (1985).